MagneTrack: Magnetic Field Separation Method for Continuous and Simultaneous 1-DOF Tracking of Two-magnets

Takehiro Abe
Independent
Kyoto, Kyoto, Japan

Daisuke Sakamoto
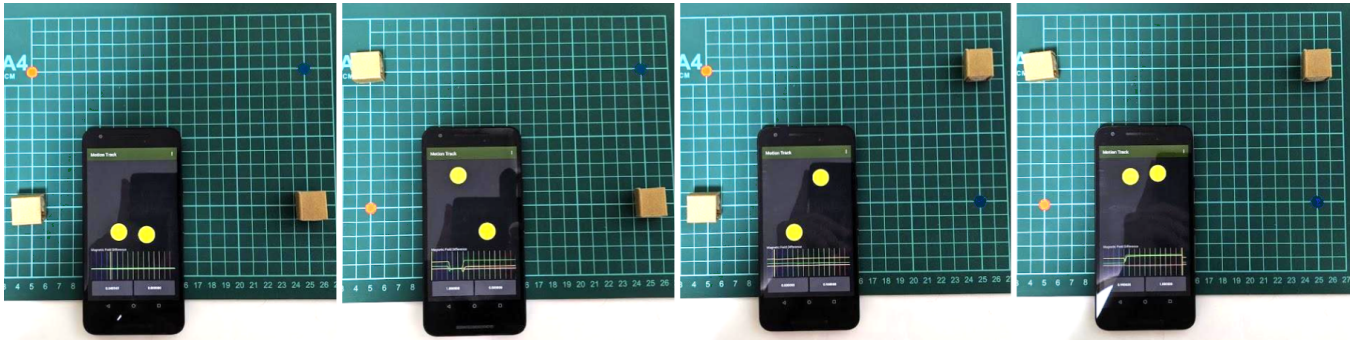Hokkaido University
Sapporo, Hokkaido, Japan

Figure 1: Tracking two magnets individually using a common smartphone on straight lines.

ABSTRACT

This paper presents a method to track two magnets using one magnetometer on a smart device (e.g., smartphone), which detects the locations of the magnets around the device. A magnetometer measures the overlapping data signals generated by the two magnets. Thus, a data-separation technique is required to separately track the continuous and simultaneous signals generated by the two magnets. In this study, we develop a separation algorithm based on nonnegative matrix factorization to continuously and simultaneously track two magnets, and then conduct an experiment to validate our concept. We then compare our method in both simulated and actual environments. In the actual environment, we observe real data signals arising from the two magnets on a magnetometer. Finally, we present example applications to demonstrate the use cases of our model in human–computer interaction systems.

CCS CONCEPTS

• **Human-centered computing** → **Smartphones**; **User interface design**; **Human computer interaction (HCI)**.

KEYWORDS

magnetic user interface, magnetic field separation, algorithm, two-magnet tracking

1 INTRODUCTION

Magnets are important materials used in human–computer interaction (HCI) research; they are small and cheap, but powerful enough to demonstrate various user interactions. Researchers have used this material to track finger movements around a smartphone and smartwatch [10, 15], tangible and physical interactions [24, 27], and midair interaction [22]. In addition to interaction variations, there are various configurations of magnets and magnetometers, such as interaction with magnetometer arrays [25], multiple tangible objects with magnets [13], and spinning magnets [3]. In this paper, we focus on the configuration of one magnetometer and two magnets, and propose a method to continuously and simultaneously track the magnets' positions along straight lines around a common smart device (Fig. 1).

Continuous and simultaneous two-magnet tracking will greatly enhance physical interactions on smart devices. The input range of the touchscreen used as an input interface for smart devices depends on its size. The larger the screen, the larger the input range; however, this reduces the device's portability. In contrast, the smaller the screen, the better the portability; however, this makes touch interactions difficult. Therefore, an auxiliary input widget, independent of the screen size, can be added to a smart device to make it more user friendly. In particular, continuous input widgets, such as sliders and levers, are highly compatible with

a conventional swiping operation (e.g., screen scrolling); consequently, they are easier to use than discrete input components, such as buttons. Furthermore, continuous input devices are well suited to tangible user interfaces and game controllers, and can thus enhance the functionality of smart devices. One advantage of using magnets with smart devices is that many such devices have built-in magnetometers; therefore, our concept of continuous and simultaneous two-magnet tracking does not require any hardware modification.

To develop a continuous and simultaneous two-magnet tracking method, we employ a magnetic field-separation approach. Some machine-learning algorithms widely used in HCI, such as random forest and support vector regression, are suitable candidates for magnet-tracking problems. However, these algorithms are used with either discontinuous positional relations or single continuous magnet tracking. For magnetic field separation, we use a supervised learning method based on nonnegative matrix factorization (NMF). NMF is often used for tasks involving both image and audio signal processing [21, 31], and it is also effective for magnetic field separation, which has similar properties.

We formulate a method to separate the overlapping magnetic fields from one magnetometer to track two magnets on straight lines. Our model tracks magnets on one-dimensional (1D) straight lines on two sides of the magnetometer. Although this method is only 1D, it is the first approach proposed to separate overlapping magnetic fields using NMF. We develop an algorithm to realize magnetic field separation and develop a prototype system to establish our concept.

The contributions of our work are summarized as follows:

(1) We develop an algorithm to realize continuous and simultaneous two-magnet tracking by separating the overlapping magnetic fields. For this purpose, only a three-point calibration process is necessary; our method does not require much data for learning.

(2) We validate our method by comparing the results in both simulated and actual environments. In the actual environment, we observe the data obtained from a magnetometer in response to the two magnets.

(3) We demonstrate example applications to illustrate the use case of our technique.

2 RELATED WORK: MAGNETIC USER INTERFACE

Various magnetic user interfaces have been proposed to date for both input to output. For output interfaces, due to the attraction and repulsion properties of magnetic materials, some researchers have explored the application of magnets to haptic feedback [5, 27, 30, 36–38, 42]. In contrast, we focus on the application of magnets as input interfaces that operate by continuously and simultaneously tracking two magnets placed around a smart device.

2.1 Single-Magnet Tracking

Most modern smart devices are equipped with a magnetometer; thus, many input interfaces using the magnetometer have been proposed. Harrison and Hudson proposed an approach to start software apps by detecting the difference in the magnetic field generated by a magnet attached to the user's finger [10]. Ketabdar *et al.* also proposed a gesture input system for smart devices using a magnet, which was shown to be applicable to various software apps [17, 18]. Kadomura and Siio proposed user interaction via a magnet attached to a fingernail, which was intended to allow users to operate smart devices naturally [15]. Zalmai *et al.* proposed a gesture-recognition method by fitting the trajectory model, assuming straight movement gestures [41]. Yoon *et al.* demonstrated an interesting approach that combined a magnet with an inertial measurement unit (IMU) for three-dimensional (3D) pen- and finger-based interactions [39, 40]. McIntosh *et al.* used a magnet not only for gesture input, but also for haptic feedback by placing a coil on a smart device [26]. They also utilized IMU to apply geomagnetism cancellation to improve the tracking accuracy. By using a magnetic ring, Park *et al.* identified which finger was used on the touchscreen [29]. They achieved high accuracy by applying geomagnetism cancellation and further used the touched position as a feature of machine learning.

2.2 Multimagnet Identification

Hwang and Bianchi proposed the use of tangible magnets to interact with smart devices [2, 13], and Hwang *et al.* demonstrated a tangible interaction system with multiple tangible objects using multiple magnets [13]. However, their six-page paper did not present the system implementation adequately; hence, we were unable to reconstruct it. Moreover, they neither conducted an experiment to demonstrate the system's accuracy nor provided adequate metrics to understand the system's operation. Hwang *et al.* also tried to detect the movement of a pair of magnets by using a decision tree [12]. However, this approach could only handle the static positional relation of magnets, and not continuous position tracking. To resolve this issue, Bianchi and Oakley proposed a model to recognize multiple tangibles that spin a magnet based on the frequency component of the magnetic field [4]. Although recognition based on the frequency component can work robustly, even when the number of tangibles increases, it requires special devices to spin the magnet. Chan and Gollakota proposed an interaction method using magnetic patterns generated from a conductive thread [6]. As the interference of each magnetic pattern is trivial, the problem of overlapping magnetic fields can be avoided.

2.3 Advanced Magnet Tracking Using Multiple Magnetometers

Some researchers have increased the number of magnetometers in order to detect the exact movement of a magnet. Chen *et al.* achieved 3D point tracking of a fingertip using two magnetometers, which cannot be achieved using a single magnetometer [7]. Moreover, Chen *et al.* tracked five fingers independently by increasing the number of magnetometers from two to four and using AC-driven electromagnets operating at unique frequencies [8]. Similarly, Parizi *et al.* embedded three magnetometers on a smartwatch and precisely tracked an index finger wearing an electromagnet as a ring [28]. Liang *et al.* and Kuo *et al.* recognized both the precise location and type of magnet tangibles in a smart device in which a Hall effect sensor grid was embedded [20, 23–25]. Even though a simple

algorithm can estimate the exact position of a magnet by increasing the number of sensors, this approach requires a special device, such as a magnetometer grid.

2.4 Continuous and Simultaneous Two-Magnet Tracking: Our Contribution

Various studies were conducted on the use of magnets for user interfaces in the field of HCI. These studies demonstrated various applications using single–, double–, or multiple–magnet tracking and/or identification techniques. Among these, we focus on continuously and simultaneously tracking two magnets with one degree of freedom. Similarly, MagGetz [13], demonstrated some example applications of continuous and simultaneous magnet tracking using a similar method to ours. Our method shows advantages over theirs in terms of ease of calibration, ease of geomagnetic cancellation, and stability with respect to the relative position change of the sensor and magnet. To achieve facile calibration, we develop an algorithm to separate the overlapping magnetic fields and track two magnets using only three-point calibration. Similarly, we implemented geomagnetic cancellation so that the smart device can be used with two magnets while being able to rotate. This mechanism contributes to the stable detection of both magnets.

3 MAGNETIC FIELD-SEPARATION METHOD

Owing to the additive property of magnetic fields, overlapped magnetic fields from multiple magnets can be separated using a linear model. This property is also applicable to complex spectra, and thus the methods used in sound source separation can be applied to magnetic field separation by extending the two-dimensional spectrum components (i.e., real and imaginary parts) to a 3D magnetic field. The complex NMF proposed by Kameoka [16] *et al.*, which can express a complex spectrum by using a compact base model, is a suitable candidate for magnetic field separation. Another candidate is that proposed by Ahuja *et al.*, in which a complex spectrum is divided into positive and negative components by NMF [1]. Our method is based on both of these methods.

We developed a method to track the positions of two magnets on straight lines using one magnetometer. The key concept for continuous and simultaneous two-magnet tracking is magnetic field separation. As shown in Fig. 2, in magnetic field separation, the input has nine values measured from IMU (i.e., accelerometer, gyroscope and magnetometer). Each of those three sensors outputs three real numbers of (x, y *and* z). The output value is the intensity ratio of each magnetic field difference H_i. i is the index of the magnets. We use two magnets in this work, so i should be 0 and 1. As a result, we get the two output values with our method. Prior to the separation process, we registered the magnetic field obtained when all magnets are located at the reference position $\mathbf{d}_i^{(b)}$ and when each magnet is located at the boundary position $\mathbf{d}_i^{(e)}$ for calibration. By interpolating both positions as corner points,

$$\mathbf{d}_i = (1 - H_i)\mathbf{d}_i^{(b)} + H_i\mathbf{d}_i^{(e)}, \tag{1}$$

we estimated the position of each magnet $\mathbf{d}_i$.

(a) Calibration of separation process

(b) Calibration of geomagnetism cancellation
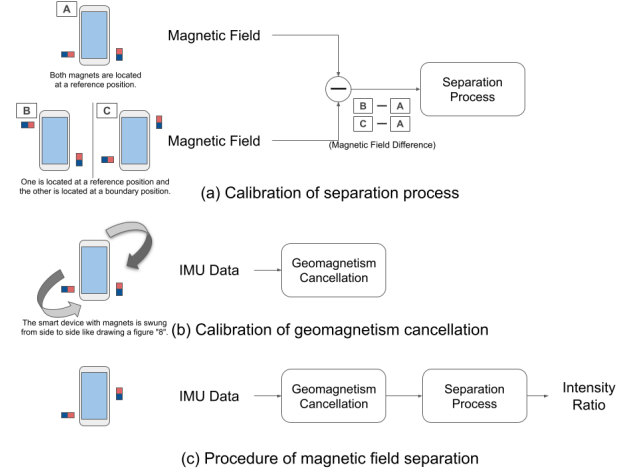
(c) Procedure of magnetic field separation

Figure 2: Overview of magnetic field separation. (a) Our separation system is calibrated with two magnetic field differences between a magnetic field observed when both magnets are located at a reference position (i.e., case A) and those observed when each magnet is located at a boundary position (i.e., case B and case C). (b) Our geomagnetism cancellation system is calibrated with the observed IMU data while the smart device with magnets is swung from side to side, similar to drawing a figure 8. (c) The output is an intensity ratio that expresses where each magnet is located between the reference and the boundary position.

3.1 Magnetic Field Difference Model

If the 3-axis indices of the magnetic field are defined as $\phi \in \{x, y, z\}$, then the difference model of the magnetic field generated from each magnet can be expressed by the product of the preregistered magnetic field difference $X_{i,\phi}$ (basis vector) and the intensity ratio of each current magnetic field H_i, as follows:

$$M_{i,\phi} = H_i X_{i,\phi}, \tag{2}$$

where H_i satisfies the condition $0 \leq H_i$. Using the magnetic field difference model $M_{i,\phi}$ and the magnetic field observed when all magnets are located at the reference position E_ϕ, the magnetic field measured from a magnetometer B_ϕ is established as follows:

$$B_\phi = \sum_i M_{i,\phi} + E_\phi + \epsilon_\phi, \tag{3}$$

where ϵ_ϕ is the error due to the model error and noise.

3.2 Geomagnetism Cancellation

E_ϕ comprises the geomagnetic field and magnetic field generated when both magnets are located at the reference position $\mathbf{d}_i^{(b)}$. When the orientation of the smart device is tilted, the positional relation between the two magnets and the magnetometer is constant, whereas the geomagnetic field component rotates depending on device orientation. Therefore, we apply a simple approach of geomagnetism cancellation, which is quite similar to that proposed

by [26]. E_ϕ is expressed as

$$E_\phi = \sum_{\phi' \in \{x,y,z\}} R_{\phi\phi'} E_\phi^{(G)} + E_\phi^{(H)}, \qquad (4)$$

using the rotation matrix of the device orientation $R_{\phi\phi'}$, which can be obtained from its accelerometer and its gyroscope, the geomagnetic field observed when the smart device is not tilted (i.e., absolute orientation) $E_\phi^{(G)}$, and the magnetic field generated from the two magnets and an environment $E_\phi^{(H)}$. The variable $E_\phi^{(H)}$ is well known as the hard iron effect in the task of geomagnetism cancellation [19, 33], which indicates an observed geomagnetic field distortion produced by a paramagnetic material, such as a permanent magnet. As shown in Eq. (4), E_ϕ is distributed on the surface of a sphere with center $E_\phi^{(H)}$ and radius $E_\phi^{(G)}$ $(= \sqrt{E_x^{(G)2} + E_y^{(G)2} + E_z^{(G)2}})$. Therefore, we sampled the magnetic field at various orientations of the smart device with two magnets for calibration, and then fitted the sphere to the sampled data $B_{k,\phi}$. Next, we applied a least-squares method where the following was used as a cost function to obtain $E_\phi^{(H)}$ and $E_\phi^{(G)}$:

$$\mathcal{J} \equiv \sum_k (\sum_\phi (B_{k,\phi} - E_\phi^{(H)})^2 - E_\phi^{(G)2})^2. \qquad (5)$$

We obtained the magnetic field difference generated from the two magnets Y_ϕ by applying geomagnetism calibration with the observation data:

$$Y_\phi = B_\phi - E_\phi. \qquad (6)$$

3.3 Separation Process

Based on NMF, we separated the magnetic field difference of two magnets Y_ϕ into those of each magnet $M_{i,\phi}$. For a real given magnetic field difference, we separated the observation data and the basis vector into positive and negative components applied to NMF.

$$Y_\phi^{(+)} = \max(0, Y_\phi), \quad Y_\phi^{(-)} = \min(0, Y_\phi) \qquad (7)$$

$$X_{i,\phi}^{(+)} = \max(0, X_{i,\phi}), \quad X_{i,\phi}^{(-)} = \min(0, X_{i,\phi}) \qquad (8)$$

Each component is assigned to the following NMF update formulas:

$$\beta_{i,\phi}^{(+)} = \frac{H_i X_{i,\phi}^{(+)}}{\sum_n H_n X_{n,\phi}^{(+)}}, \quad \beta_{i,\phi}^{(-)} = \frac{H_i X_{i,\phi}^{(-)}}{\sum_n H_n X_{n,\phi}^{(-)}}, \qquad (9)$$

$$\hat{Y}_{i,\phi}^{(+)} = H_i X_{i,\phi}^{(+)} + \beta_{i,\phi}^{(+)} (Y_\phi^{(+)} - H_i X_{i,\phi}^{(+)}),$$
$$\hat{Y}_{i,\phi}^{(-)} = H_i X_{i,\phi}^{(-)} + \beta_{i,\phi}^{(-)} (Y_\phi^{(-)} - H_i X_{i,\phi}^{(-)}), \qquad (10)$$

$$H_i = \frac{\sum_\phi (\hat{Y}_{i,\phi}^{(+)} X_{i,\phi}^{(+)} / \beta_{i,\phi}^{(+)} + \hat{Y}_{i,\phi}^{(-)} X_{i,\phi}^{(-)} / \beta_{i,\phi}^{(-)})}{\sum_\phi ((X_{i,\phi}^{(+)})^2 / \beta_{i,\phi}^{(+)} + (X_{i,\phi}^{(-)})^2 / \beta_{i,\phi}^{(-)})}. \qquad (11)$$

Eq. (9) derives the component ratio of the magnetic field generated from each magnet $\beta_{i,\phi}$, Eq. (10) distributes the difference between the observation data and the magnetic field difference model to the magnetic field model with the component ratio, and Eq. (11) calculates the intensity ratio H_i from the values obtained in Eq. (9) and Eq. (10). By iteratively updating Eq. (9), (10), and (11), the solution converges to a stationary point. Finally, the intensity ratio

of each magnetic field H_i obtained through this iteration and the position of each magnet $\mathbf{d}_i$ were derived from Eq. (1).

4 EXPERIMENT

We conducted an experiment to validate our method by comparing the results obtained in simulated and real environments. In the real environment, we obtained data from a magnetometer in response to two magnets.

4.1 Condition

We compared two conditions in this experiment: the simulated and actual environments.

4.1.1 Simulated Ideal Environment (Simulation). We tested our method in a simulated magnetic field that represented an ideal environment without any noise. All parameters in this scenario were fabricated by a Java program, and all trials were performed in the simulated environment.

4.1.2 Actual Environment (Actual). In this environment, we tested our method in a real magnetic field, which was monitored using a magnetometer, which varied in response to the movements of two magnets. All trials were performed with a magnetometer installed on a smartphone and two magnets. We collected data using various combinations of parameters in an actual environment, and then supplied the collected data to be analyzed by our method.

The following sections mainly describe the experimental setup and parameters in the actual environment. The simulated environment was created to mimic the actual environment.

4.2 Setup and Apparatus

This experiment employed two magnets, each of which comprised four small magnets (13 mm in diameter and 2.5 mm thick with a flux density of 180 mT by Seria Co., Ltd.). All four magnets were stacked to form a single cylindrical magnet. We used a Nexus 5X smartphone with an installed magnetometer as a data-recording device. The exact position of the magnetometer on board was not officially available, so we exploratively searched for its position. The yellow circle on the smartphone in Fig. 3 indicates the estimated position of the sensor. The error margin was approximately ±1 mm.

Fig. 3 shows the experimental data-collection setup, where the Nexus 5X is located in the center as the data-recording device. We adjusted its position to align the magnetometer with the center of the experimental setup. The two magnets were designed to move along straight lines on the left and right sides of the recording device. The experimental parameters are discussed in the next subsection.

4.3 Parameters

4.3.1 Direction of the Magnetic Field. A magnet creates a directional magnetic field around itself comprising three spatial dimensions (i.e., x, y and z) (Fig. 4). In this experiment, we used three variations of the parameters to determine the direction of the magnetic field. There are two lines on the z plane in the experimental setup, on the left and right sides of the device. The same direction is used for the two magnets; thus, there are nine variations of the parameters: $lx - rx$ (left-x and right-x), $lx - ry$, $lx - rz$, $ly - rx$,
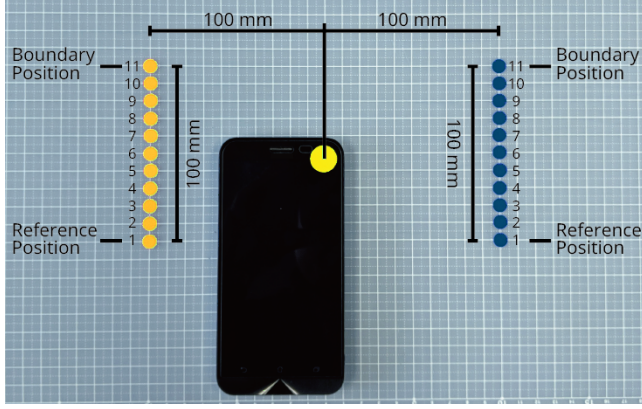
Figure 3: Environmental setup for data collection (*SensorMIDDLE*)

.

$ly - ly$, $ly - rz$, $lz - rx$, $lz - ry$ and $lz - rz$. We maintained this pair of straight lines as the two magnets moved along them.

We synthesized the magnetic field created by the two magnets and analyzed it using a magnetometer by employing the Biot–Savart law.

$$B_\phi = \frac{\mu_0}{4\pi} \left(\frac{3\langle \mathbf{m}, \mathbf{r}\rangle r_\phi}{\|\mathbf{r}\|^5} - \frac{m_\phi}{\|\mathbf{r}\|^3} \right) \tag{12}$$

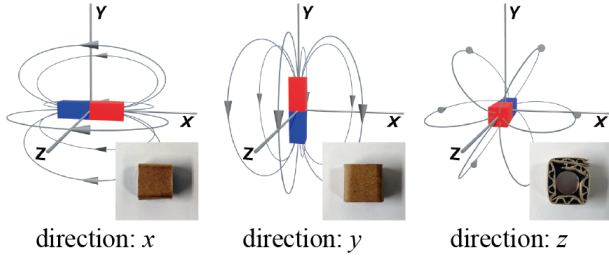direction: x direction: y direction: z

Figure 4: Direction of magnet.

4.3.2   Position of the Magnets. In this experiment, two magnets moved along straight lines. A 100-mm line was divided into 10 intervals to create 11 data points. All intervals were 10 mm wide and equally spaced (Fig. 3). We collected all combinations of left and right data points on two lines and arrived at $11 \times 11 = 121$ data points for each pair of magnet directions.

4.3.3   Position of the Magnetometer. Not only the direction of each magnet, but also the reference and the boundary positions determine the basis vector. As shown in Fig. 5, we conducted this experiment for the two positional conditions of the magnetometer described below.

(1) *SensorMIDDLE*: A magnetometer is located at the middle of the magnets' movement range. *SensorMIDDLE* is a condition in which the distance between the magnet and magnetometer is equal when the magnet is placed at the reference or boundary position.

(2) *SensorTOP*: A magnetometer is located at the top of the magnets' movement range. *SensorTOP* is a condition in which the distance between the magnet and magnetometer simply decreases as the magnet moves from the reference position to the boundary position.

We selected those two conditions to investigate how the line and magnetometer positions affect the tracking results. The *SensorMIDDLE* condition is a balanced case where the distances between the sensor and both the boundary and reference positions are equal, and *SensorTOP* condition is an unbalanced case. These conditions are considered because the distances between the magnets and the sensor are important factors in this experiment. Our hypothesis is that the unbalanced case will more robustly track magnets than the balanced case because the position is not uniquely determined when the distance is symmetrical. Note that we only select one condition for the unbalanced case, and omit the corresponding *SensorBOTTOM* case because the *SensorTOP* and *SensorBOTTOM* are symmetric in terms of the distance between the magnets and sensor. Thus, their results should be the same.
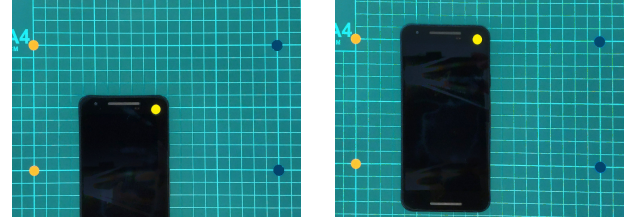
SensorMIDDLE.   *SensorTOP.*

Figure 5: Positional conditions of magnetometer.

4.4   Procedure

The experimental procedure is as follows:

(1) The magnetometer location was selected based on the positional conditions *SensorMIDDLE* and *SensorTOP*.

(2) A pair of directions was selected for the two magnets.

(3) The device was calibrated by first placing the two magnets on the reference positions, and then recording the positions on the device. Second, the left magnet was moved to the boundary position on the left line and the two magnet positions were recorded. Third, the left magnet was returned to the reference position on the left line, the right magnet was moved to the boundary position on the right line, and the two magnet positions were recorded.

(4) Data collection commenced from the reference positions. We collected $11 \times 11 = 121$ data points by fixing the directions of the magnets while moving them along the straight lines.

(5) Steps 1–4 of the procedure were repeated until all two positional conditions and all nine pairs of direction of the magnets were completed. Note that the order of selection in these steps did not affect the experimental result.

We performed the above procedure for data collection in a real environmental setup. Data collection was completed in four hours. In contrast, the magnet position tracking was conducted within, at most, 10 ms.

4.5 Results and Discussions

4.5.1 Results. Fig. 6 shows the results of the experiments conducted in the simulated and actual environments. Two results were obtained for each dataset because there are two sets of magnets and lines. The orange color represents the results of the left side of the magnet, and the navy color represents the results of the right side of the magnet. The color strength signifies the proximity of the magnet on the line to the reference position, where white represents 0 mm from the reference position and the full color represents 100 mm from the reference position. The results are represented as a matrix, which shows all combinations of the positions of the two magnets (Fig. 7).

Fig. 8 shows the mean absolute errors between the two results from the simulated and real environments. The error indicates the difference between the simulated and actual positions; the lower the error, the better the results. The minimum error is zero. In *SensorMIDDLE*, there are two pairs that show a small error in both the left and right lines: $lx-ry$ and $ly-rx$. In contrast, in *SensorTOP*, all pairs show smaller errors along both the left and right lines compared to those of the *SensorMIDDLE* condition. These results indicate that our method successfully calculates the actual positions from the observation of a magnetometer, depending on the combination of the magnet direction and positional conditions.
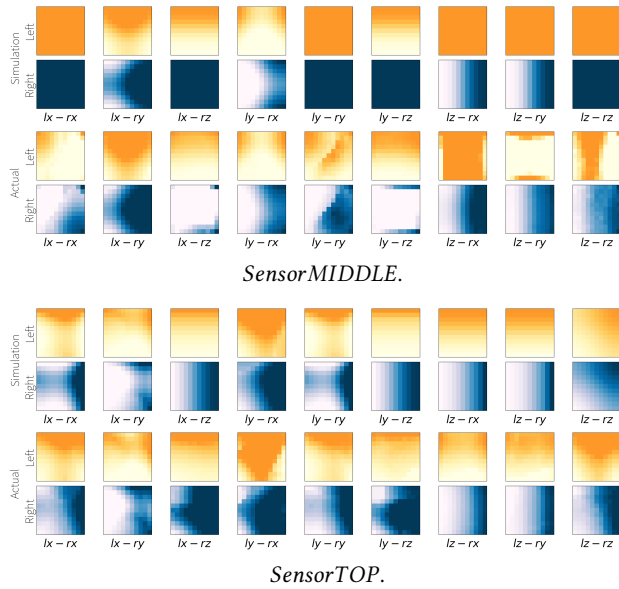

SensorMIDDLE.

SensorTOP.

Figure 6: Results of the simulated (top) and actual (bottom) environments
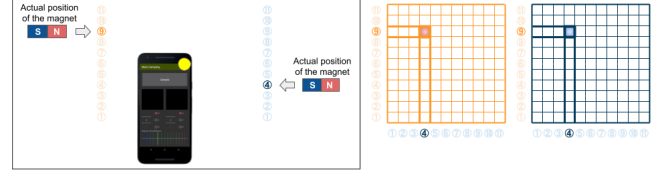

Figure 7: Visualization method for the collected data.

4.5.2 Discussion. Here, we briefly discuss the reason for the differences between the *SensorMIDDLE* and *SensorTOP* conditions. The key difference arises from the relationship between each magnet and the magnetometer. Fig. 9 shows the differences in the magnetic field when each magnet is moving along a straight line in the simulated environment. As we can see from the two basis vectors of the z direction in *SensorMIDDLE* (Fig. 9 left side), all the components of magnetic field at the boundary position are zero; therefore, the basis vector $X_{i,\phi}$ is zero. This is because the distances between the magnetometer and both the reference and boundary positions are the same in the case of *SensorMIDDLE*. The relative position from a magnet to a magnetometer on the z-plane is $\mathbf{r} = (x_0, y_0, 0)$, and the moment of a magnet which is directed to z is $\mathbf{m} = (0, 0, m_0)$; thus, the inner product of the two vectors is zero: $\langle \mathbf{m}, \mathbf{r} \rangle = 0$. Substituting this zero value into Eq. (12) yields $B_\phi = -\frac{m_\phi}{\|\mathbf{r}\|^3}$, which only includes the moment of the magnet and the distance between the magnet and magnetometer. Because the magnet moment is always constant, the magnetic field difference at the reference position is equal to that at the boundary position (i.e., $Y_\phi = 0$ when each magnet is placed at either of the two positions). In contrast, the distance between the magnet and the magnetometer is not the same at every point between the reference and boundary positions in the case of *SensorTOP*; therefore, the basis vector $X_{i,\phi}$ is not zero, and the algorithm more accurately separates the magnetic field than in the case of *SensorMIDDLE*.

In addition to the case of the z direction in *SensorMIDDLE*, when two magnets point to the same direction (i.e., $lx - rx$, $ly - ry$ and $lz - rz$), our method could not track each magnet at all. This is because the observed magnetic field difference Y_ϕ cannot be uniquely recombined from the basis vector $X_{i,\phi}$. As shown in "direction: x" of Fig. 9, the basis vectors of two magnets in *SensorMIDDLE* are $X_{left,\phi} = (0, B_y, 0)$ and $X_{right,\phi} = (0, -B_y, 0)$, respectively. Thus, the basis vectors are parallel. For example, if a magnetic field difference $Y_\phi = (0, B_y, 0)$ is observed, this can induce a nonunique intensity ratio: $(H_{left}, H_{right}) = (1.0 + \alpha, \alpha)$. This is also applicable to "direction: y" and "direction: z" (note that first of all, the basis vector of the "direction: z" becomes zero).

From the above discussion, we conclude that the key to accurate tracking is ensuring that the basis vectors are asymmetric. As can be seen from the two basis vectors of the x direction in *SensorTOP* (Fig. 9 right side), the basis vectors need not be fully orthogonal to achieve accurate tracking. This is because the error of $lx - rx$ in *SensorTOP* is not high, even though there is only a small difference in the y component between these basis vectors. This is
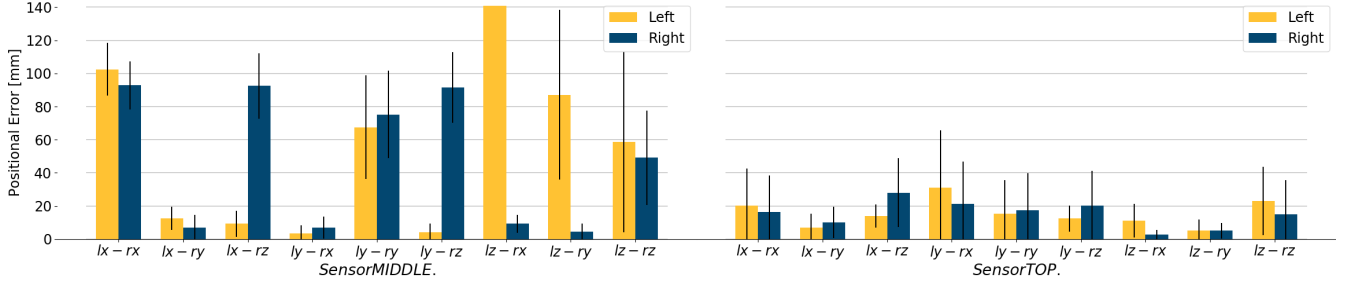
Figure 8: Average and standard deviation (SD) of the errors.

Case of moving left magnet for *SensorMIDDLE*.

Case of moving left magnet for *SensorTOP*.

Case of moving right magnet for *SensorMIDDLE*.
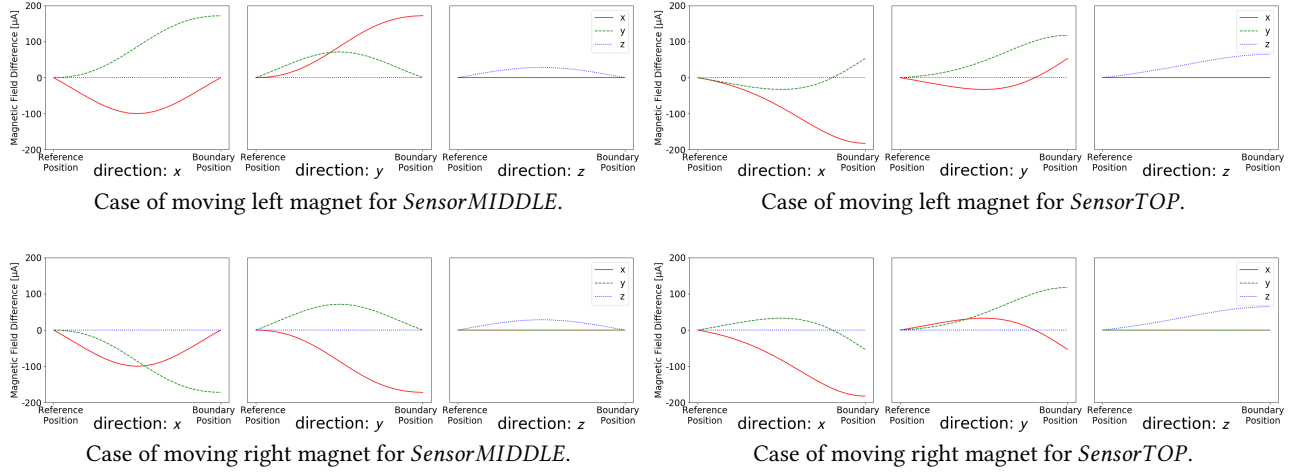
Case of moving right magnet for *SensorTOP*.

Figure 9: Magnetic field difference simulated while each magnet is moved between the reference and boundary positions.

likely to be satisfied in *SensorTOP* based on these results. In addition, as mentioned above, the distance between the magnetometer and a magnet in *SensorTOP* simply decreases in response to the magnet's movement. Therefore, *SensorTOP* is a position condition where the magnetic field changes more linearly with respect to magnet movement than in *SensorMIDDLE*. NMF is a model that assumes linearity, and *SensorTOP* also meets this assumption better than *SensorMIDDLE*. Therefore, we recommend placing the sensor in an unbalanced location in terms of the distance between the magnets and the sensor. Theoretically, a sensor can be placed at *SensorRIGHT* or *SensorLEFT*, because the position is geometrically same as *SensorTOP* in this setup. If the positional relationship between the magnets and sensor becomes more unbalanced, then the system can robustly and accurately track the magnets.

It has been demonstrated clearly that our algorithm performs well in the continuous and simultaneous tracking of two magnets in *SensorTOP*, regardless of the combination of magnet directions, but not in *SensorMIDDLE*, except in the case where the combination of magnet directions is x *and* y. The proposed magnetic field-separation method was the first algorithm to track two magnets in this manner; we implemented and demonstrated its viability for the HCI applications in this study. Previous studies on magnet tracking for user interface applications (e.g., [13]) did not aim to

evaluate how their systems work. In contrast, our work is the first attempt to evaluate the continuous and simultaneous two magnet tracking algorithm.

5 EXAMPLE APPLICATIONS

We created several example applications to examine the effectiveness of our method. Our algorithm tracks two magnets on two lines with a magnetometer, which has three axes (x, y *and* z). Our experiment uses the x and y axes on the z plane, but the result is not limited to them. We can also use this method with other axes (i.e., x *and* z or y *and* z) via simple calibration. Similarly, our algorithm works if the magnets move in two orthogonal lines; the two magnets do not necessarily need to be on the same plane. The system will separate the magnetic field for two orthogonal lines, as well as for lines on the same planar surface. The examples discussed below use various axes.

5.1 Smartphone Case with Input Assistance

Our method can be applied to a smartphone case that has mechanical widgets, such as that presented in [34]. We created a simple web browsing app as a use case. As shown in Fig. 10, the smartphone case has two physical sliders: one that can move vertically and another that can move horizontally. The user is expected to

Figure 10: Web browsing app: (a) the smartphone case has a top slider and a side slider that each include a magnet unit, (b) the back of a smartphone with the case, (c) pulling the top slider, (d) scrolling a website down by pulling the top slider, (e) scrolling a website up by pressing the side slider, and (f) zooming a website by pulling the top slider and pressing the side slider simultaneously.

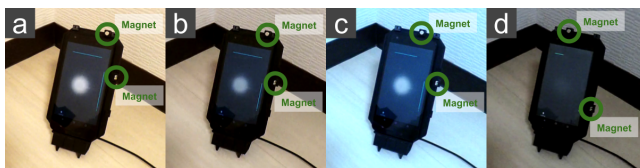Figure 11: Music and dance game (©SAN-X CO., LTD).

Figure 12: Ambient light control: (a) the smartphone stand has a top slider and a right slider that each includes a magnet unit, (b) moving the right slider down to make the illuminance dark, (c) moving the top slider to the left side to make the ambient color blue, (d) moving the right slider to the bottom side to turn the ambient light off.

manipulate these sliders with the index finger and thumb, respectively. Each slider has a 3D-printed spring that is similar to the mechanism proposed in [35]. In essence, except for the attached
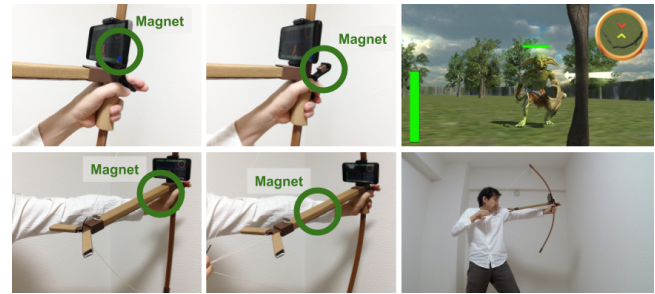

Figure 13: Archery game.

magnets, this smartphone case was made entirely of a 3D-printed filament. When the vertical slider is pulled, the app screen scrolls down. When the horizontal slider is pushed, the app screen scrolls up. Furthermore, when both sliders are triggered, the app screen zooms in to the center. Although these operations are also feasible through gestures on a touch screen, such as swiping and pinching, the smartphone case can adjust the scrolling speed continuously without occlusion.

5.2 Game Controller: Stuffed Toy Arms

We created an example application that detects the vertical position of a stuffed toy's arms (Fig. 11), with which the users can manipulate two objects on the screen. The arms can regulate the input from the users through vertical movements along straight lines; this is an intuitive example of using continuous and simultaneous two-magnet tracking in practical usage. Beyond the simple manipulation of a stuffed toy, we also created a music and dance app in which a user makes the stuffed toy dance. Here, musical notes are displayed based on the movement of the toy's arms. Our method can the track continuous positions of the hands of the stuffed toy, thus allowing a user to input two movements more easily than by using a conventional game controller. It is also possible to imagine various other applications for games, such as fighting virtual enemies and moving virtual objects by manipulating a real stuffed toy.

5.3 Remote for Ambient Light Control

To demonstrate more accurate tracking, we created another example application for controlling ambient light (Fig. 12). A smartphone stand is placed with two straight lines around it, and on which two magnets are placed. One magnet moves up and down along the vertical line, and the other moves left and right, like a slider, along the horizontal line. This is an orthogonal setup. Once a smartphone is set on the stand, the user first calibrates the magnets. Then, the user can control the color and illuminance level by moving the magnets along the straight lines. Our algorithm accurately tracks the position of the magnet so that the user can control the color and illuminance level intuitively. The advantage of this method is that the user does not need to calibrate the sensor frequently, as the positional relationship between the magnets and the sensor does not change frequently in everyday use.

5.4 Game Controller: Archery

Our method can be applied not only to a stuffed toy, but also to any object that allows the magnet position to be changed. As shown in Fig. 13, we created an example application in which a user can make a game character move and shoot an arrow in a virtual world corresponding to input from a bow controller. This bow controller has a grip to move one magnet to the front and a structure to move another magnet to the back by drawing the installed string. When a user does not exert a force on the controller, these magnets return to their original location via the movement of a spring and rubber thread. The virtual character's movement speed (i.e., walking, running) corresponds to the user's grip force, and the arrow action (e.g., flying distance or launch cancellation) corresponds to the user's draw force. In addition, the perspective in the virtual world can be controlled by the controller's tilt angle, which is measured by a gyroscope.

6 DISCUSSION

We summarize the experiment as follows:

- We confirmed that our method can stably track two magnets that move along straight lines on the z plane continuously and simultaneously in the case where the combination of magnet directions is x and y (i.e., $lx - ry$ or $ly - rx$) in the $SensorMIDDLE$ case.
- When the magnetometer is located outside the range of magnet movement (i.e., $SensorTOP$ in our experiment), the accuracy of tracking remains stable, regardless of the combination of magnet directions.

Here, we briefly discuss the geomagnetism cancellation and calibration process used, and the limitations of our method.

6.1 Geomagnetism Cancellation

The purpose of geomagnetism cancellation is to mitigate the influence of a geomagnetic field. Recently, geomagnetism cancellation has become a standard technique in HCI-related research fields, and our method adopts a simple method that is equivalent to those in [26, 28, 29]. Thus, the tracking accuracy is preserved, even user are likely to tilt their smart devices. This means that geomagnetism cancellation contributes to the practical application of continuous two-magnet tracking. In conventional research [13], geomagnetism cancellation was not considered because the placement of the smartphone was assumed to be fixed. However, we assume that users will tilt and swing their smart devices, even while our method is being applied, so the simple method of geomagnetism cancellation, which has been deemed effective in [26], is integrated into our method. Although there was no detailed procedure was provided for geomagnetism cancellation calibration, we used a well-known calibration procedure used on Google Maps: sampling IMU data while the smart device is swung from side to side, similar to drawing a figure 8.

In geomagnetism cancellation, we and [26, 28] assume that there is no distortion in the observed geomagnetic field, and simply rotate the premeasured geomagnetic field according to the tilt of the smart device. Thus, the distribution of geomagnetism in $(x, y \text{ and } z)$ is assumed to be spherical. Although Park *et al.* account for the distortion by updating the premeasured geomagnetic field constantly when no magnets are nearby [29], the model of the geomagnetic field is essentially spherical, similar to the case of our model. In contrast, it is known that the geomagnetic field distribution in $(x, y \text{ and } z)$ can become an ellipsoid due to distortion arising from the soft iron effect from ferromagnetic materials, such as steel [19, 33]. In our preliminary experiments, we also modeled the geomagnetic field as an ellipsoid, but the tracking accuracy did not improve significantly, whereas the increased parameters (e.g., three elliptic radii) increased the overfitting. Therefore, we adopted the simpler method proposed by [26, 28]. In robotics, to improve the accuracy of a robot's position recognition, machine learning-based methods, such as the Bayesian nonparametric model [32], neural networks, and support vector regression [9], have been proposed to better model the distribution. The complexity of these models makes them unsuitable for input user interfaces because they require considerable data input for calibration (i.e., training).

6.2 Calibration

We used a simple three-point calibration technique in order to define the two straight line segments where each magnet moves within the tracking range. Such calibration is required, even in most other magnet-tracking methods. For the separation process, calibration is essential to accurately track a magnet before using a system. It is used not only for two-magnet tracking, but also for single-magnet tracking. Frequent calibration is costly for users. The total number of registrations in our method is only three: one case where both magnets are located at the reference positions, and two cases where each magnet is located at a boundary position. This number of registrations is the same as that used in other conventional research [13].

As shown in Fig. 2, the calibration of our method consists of two mutually independent parts: one for the separation process and the other for geomagnetism cancellation. That means there is no need to calibrate the separation process again when geomagnetism cancellation is recalibrated, and vice versa. The separation process requires recalibration when either the range of magnet movement, magnet orientation, or type of magnet to be tracked is changed. For example, a user needs to recalibrate the separation process when they change their application from a game controller (Section 5.2) to a smartphone case (Section 5.1). Because the observed geomagnetism is susceptible to building materials (e.g., ferromagnetic materials) [32], the geomagnetism cancellation is recommended to be recalibrated when changing rooms.

The deep neural network (DNN) is a major option for the source-separation task that has been researched previously [11, 14]. DNN is a more widely used technique than NMF; however, it requires a considerable amount of training data to track the magnets accurately and stably. In contrast, our source-separation algorithm based on the NMF requires only three data for continuous and simultaneous magnet tracking, which is significantly less than that required by the DNN. This simplifies the calibration process, which is also better for the end-users. We consider that the calibration process of our technique is easy enough for practical use.

6.3 Limitations

Observing the magnetic field generated from magnets far away from a sensor is difficult because the intensity of a magnetic field is inversely proportional to the square of the distance. A strong magnet can help reduce this limitation; however, it is difficult to use due to safety concerns, as strong magnets can break electric appliances. Therefore, it is difficult to apply our method to large-scale, full-body interactions. Moreover, this limitation does not only apply to our algorithm and method, but also to all models using magnets in general. Similarly, our method cannot track magnets if they stray from the line between the reference and boundary positions.

Our model tracks two magnets along two straight lines with 1 degree of freedom (DoF), which is simply a theoretical constraint that is the same as in previous research conducted in the field of HCI. As the value measured from the magnetometer of a smart device comprises three continuous values (i.e., 3 axes), a single magnetometer can only identify the status of a magnet with less than three DoFs. In theory, tracking three magnets on straight lines seems to be feasible; however, it requires a rigid positional condition to be found where each basis vector of the three magnets is nonzero and different in value. We and previous researchers [4, 13], who have proposed models to identify or track multiple magnets using only a single magnetometer, are subjected to this limitation. Therefore, in multimagnet tracking using a common smart device, the capability of each magnet-tracking task should be 1 DoF. Regardless of this limitation, Hwang *et al.* demonstrated many example applications using the combination of either one slider, one rotation knob, or two buttons [13]. Additionally, we demonstrate three example applications of continuous two-magnet tracking using two sliders or two game controller levers. Similarly, our method can reproduce all the example applications presented in [13] by simply adding a threshold for the tracking result obtained as continuous values.

Because our method uses one magnetometer to track two magnets, the effect when a magnet strays from a straight line is significant; therefore, it affects the tracking results of not only the magnet that the user is moving, but also the other. For example, in the example using a stuffed toy's arms (Fig. 11), when the left arm of the toy strays from a straight line in an unintended direction, the system still assumes that the magnet on the line. As a result, the system misunderstands the position of both the left and right sides. This suggests that the position of the left magnet affects the position of the right magnet. Hence, our method requires either a physical mechanism to keep the movement of each magnet on a straight line or a design that guides the user to move each magnet along a straight line. A magnetometer array, as proposed in [24, 25], can also track each magnet moving along a straight line. This method is capable of tracking a magnet moving on a plane as well as on a straight line, but it is also superior in terms of tracking each magnet independently; therefore, if a magnet moves away from a straight line, the other magnet is not affected.

Thus, our work has a limitation in that the system may misunderstand the position of both magnets because we use a single sensor for our method, which is otherwise an advantage and a key contribution of our work. It is currently difficult to install two magnetometer sensors on a smartphone. Although our method requires large constraints to use, the algorithm used in our method continuously and simultaneously tracks two magnets stably while they remain on the straight lines. Our example applications demonstrated the possibility of utilizing our single-magnet method, and we believe that our work provides new insights into magnetic HCI research.

7 CONCLUSION

We presented a method to continuously and simultaneously track the positions of two magnets around a common smart device. The key concept underlying our method is using NMF to separate the overlapping magnetic fields observed by the magnetometer on a smart device. We conducted an experiment to validate our method by comparing a simulated ideal environment and an actual environment. The two pairs of magnet directions were successfully separated, and their positions were accurately tracked by our method in an actual environment with a smart device.

REFERENCES

[1] Chaitanya Ahuja, Karan Nathwani, and Rajesh M. Hegde. 2014. A Complex Matrix Factorization approach to Joint Modeling of Magnitude and Phase for Source Separation. *CoRR* abs/1411.6741 (2014). arXiv:1411.6741 http://arxiv.org/abs/1411.6741

[2] Andrea Bianchi and Ian Oakley. 2013. Designing Tangible Magnetic Appcessories. In *Proceedings of the 7th International Conference on Tangible, Embedded and Embodied Interaction* (Barcelona, Spain) *(TEI '13)*. ACM, New York, NY, USA, 255–258. https://doi.org/10.1145/2460625.2460667

[3] Andrea Bianchi and Ian Oakley. 2015. MagnID: Tracking Multiple Magnetic Tokens. In *Proceedings of the Ninth International Conference on Tangible, Embedded, and Embodied Interaction* (Stanford, California, USA) *(TEI '15)*. ACM, New York, NY, USA, 61–68. https://doi.org/10.1145/2677199.2680582

[4] Andrea Bianchi and Ian Oakley. 2015. MagnID: Tracking Multiple Magnetic Tokens. In *Proceedings of the Ninth International Conference on Tangible, Embedded, and Embodied Interaction* (Stanford, California, USA) *(TEI '15)*. ACM, New York, NY, USA, 61–68. https://doi.org/10.1145/2677199.2680582

[5] Roger Boldu, Sambhav Jain, Juan Pablo Forero Cortes, Haimo Zhang, and Suranga Nanayakkara. 2019. M-Hair: Creating Novel Tactile Feedback by Augmenting the Body Hair to Respond to Magnetic Field. In *Proceedings of the 32nd Annual ACM Symposium on User Interface Software and Technology* (New Orleans, LA, USA) *(UIST '19)*. Association for Computing Machinery, New York, NY, USA, 323–328. https://doi.org/10.1145/3332165.3347955

[6] Justin Chan and Shyamnath Gollakota. 2017. Data Storage and Interaction Using Magnetized Fabric. In *Proceedings of the 30th Annual ACM Symposium on User Interface Software and Technology* (Québec City, QC, Canada) *(UIST '17)*. ACM, New York, NY, USA, 655–663. https://doi.org/10.1145/3126594.3126620

[7] Ke-Yu Chen, Kent Lyons, Sean White, and Shwetak Patel. 2013. uTrack: 3D Input Using Two Magnetic Sensors. In *Proceedings of the 26th Annual ACM Symposium on User Interface Software and Technology* (St. Andrews, Scotland, United Kingdom) *(UIST '13)*. ACM, New York, NY, USA, 237–244. https://doi.org/10.1145/2501988.2502035

[8] Ke-Yu Chen, Shwetak N. Patel, and Sean Keller. 2016. Finexus: Tracking Precise Motions of Multiple Fingertips Using Magnetic Sensing. In *Proceedings of the 2016 CHI Conference on Human Factors in Computing Systems* (San Jose, California, USA) *(CHI '16)*. Association for Computing Machinery, New York, NY, USA, 1504–1514. https://doi.org/10.1145/2858036.2858125

[9] L. Christensen, M. Krell, and F. Kirchner. 2017. Learning magnetic field distortion compensation for robotic systems. In *2017 IEEE/RSJ International Conference on Intelligent Robots and Systems (IROS)*. 3516–3521.

[10] Chris Harrison and Scott E. Hudson. 2009. Abracadabra: Wireless, High-precision, and Unpowered Finger Input for Very Small Mobile Devices. In *Proceedings of the 22Nd Annual ACM Symposium on User Interface Software and Technology* (Victoria, BC, Canada) *(UIST '09)*. ACM, New York, NY, USA, 121–124. https://doi.org/10.1145/1622176.1622199

[11] Po-Sen Huang, Minje Kim, Mark Hasegawa-Johnson, and Paris Smaragdis. 2014. Deep learning for monaural speech separation. In *2014 IEEE International Conference on Acoustics, Speech and Signal Processing (ICASSP)*. 1562–1566. https://doi.org/10.1109/ICASSP.2014.6853860

[12] Sungjae Hwang, Myungwook Ahn, and Kwangyun Wohn. 2013. Magnetic Marionette: Magnetically Driven Elastic Controller on Mobile Device. In *Proceedings of the Companion Publication of the 2013 International Conference on Intelligent*

User Interfaces Companion (Santa Monica, California, USA) *(IUI '13 Companion)*. ACM, New York, NY, USA, 75–76. https://doi.org/10.1145/2451176.2451207

[13] Sungjae Hwang, Myungwook Ahn, and Kwang-yun Wohn. 2013. MagGetz: Customizable Passive Tangible Controllers on and Around Conventional Mobile Devices. In *Proceedings of the 26th Annual ACM Symposium on User Interface Software and Technology* (St. Andrews, Scotland, United Kingdom) *(UIST '13)*. ACM, New York, NY, USA, 411–416. https://doi.org/10.1145/2501988.2501991

[14] Andreas Jansson, Eric J. Humphrey, Nicola Montecchio, Rachel M. Bittner, Aparna Kumar, and Tillman Weyde. 2017. Singing Voice Separation with Deep U-Net Convolutional Networks.. In *Proceedings of the 18th International Society for Music Information Retrieval Conference*. ISMIR, Suzhou, China, 745–751. https://doi.org/10.5281/zenodo.1414934

[15] Azusa Kadomura and Itiro Siio. 2015. MagNail: User Interaction with Smart Device Through Magnet Attached to Fingernail. In *Adjunct Proceedings of the 2015 ACM International Joint Conference on Pervasive and Ubiquitous Computing and Proceedings of the 2015 ACM International Symposium on Wearable Computers* (Osaka, Japan) *(UbiComp/ISWC'15 Adjunct)*. ACM, New York, NY, USA, 309–312. https://doi.org/10.1145/2800835.2800859

[16] Hirokazu Kameoka, Nobutaka Ono, Kunio Kashino, and Shigeki Sagayama. 2009. Complex NMF: A new sparse representation for acoustic signals. In *2009 IEEE International Conference on Acoustics, Speech and Signal Processing*. 3437–3440. https://doi.org/10.1109/ICASSP.2009.4960364

[17] Hamed Ketabdar, Amirhossein Jahanbekam, Kamer Ali Yuksel, Tobias Hirsch, and Amin Haji Abolhassani. 2011. MagiMusic: Using Embedded Compass (Magnetic) Sensor for Touch-less Gesture Based Interaction with Digital Music Instruments in Mobile Devices. In *Proceedings of the Fifth International Conference on Tangible, Embedded, and Embodied Interaction* (Funchal, Portugal) *(TEI '11)*. ACM, New York, NY, USA, 241–244. https://doi.org/10.1145/1935701.1935749

[18] Hamed Ketabdar, Kamer Ali Yüksel, and Mehran Roshandel. 2010. Magi-Tact: Interaction with Mobile Devices Based on Compass (Magnetic) Sensor. In *Proceedings of the 15th International Conference on Intelligent User Interfaces* (Hong Kong, China) *(IUI '10)*. ACM, New York, NY, USA, 413–414. https://doi.org/10.1145/1719970.1720048

[19] M. Kok and T. B. Schön. 2016. Magnetometer Calibration Using Inertial Sensors. *IEEE Sensors Journal* 16, 14 (2016), 5679–5689.

[20] Han-Chih Kuo, Rong-Hao Liang, Long-Fei Lin, and Bing-Yu Chen. 2016. Gauss-Marbles: Spherical Magnetic Tangibles for Interacting with Portable Physical Constraints. In *Proceedings of the 2016 CHI Conference on Human Factors in Computing Systems* (San Jose, California, USA) *(CHI '16)*. Association for Computing Machinery, New York, NY, USA, 4228–4232. https://doi.org/10.1145/2858036.2858559

[21] Daniel D. Lee and H. Sebastian Seung. 1999. Learning the parts of objects by nonnegative matrix factorization. *Nature* 401 (1999), 788–791.

[22] Jinha Lee, Rehmi Post, and Hiroshi Ishii. 2011. ZeroN: Mid-air Tangible Interaction Enabled by Computer Controlled Magnetic Levitation. In *Proceedings of the 24th Annual ACM Symposium on User Interface Software and Technology* (Santa Barbara, California, USA) *(UIST '11)*. ACM, New York, NY, USA, 327–336. https://doi.org/10.1145/2047196.2047239

[23] Rong-Hao Liang, Liwei Chan, Hung-Yu Tseng, Han-Chih Kuo, Da-Yuan Huang, De-Nian Yang, and Bing-Yu Chen. 2014. GaussBricks: Magnetic Building Blocks for Constructive Tangible Interactions on Portable Displays. *ACM SIGCHI Conference on Human Factors in Computing Systems (ACM CHI 2014)* (04 2014). https://doi.org/10.1145/2556288.2557105

[24] Rong-Hao Liang, Kai-Yin Cheng, Liwei Chan, Chuan-Xhyuan Peng, Mike Y. Chen, Rung-Huei Liang, De-Nian Yang, and Bing-Yu Chen. 2013. GaussBits: Magnetic Tangible Bits for Portable and Occlusion-free Near-surface Interactions. In *Proceedings of the SIGCHI Conference on Human Factors in Computing Systems* (Paris, France) *(CHI '13)*. ACM, New York, NY, USA, 1391–1400. https://doi.org/10.1145/2470654.2466185

[25] Rong-Hao Liang, Kai-Yin Cheng, Chao-Huai Su, Chien-Ting Weng, Bing-Yu Chen, and De-Nian Yang. 2012. GaussSense: Attachable Stylus Sensing Using Magnetic Sensor Grid. In *Proceedings of the 25th Annual ACM Symposium on User Interface Software and Technology* (Cambridge, Massachusetts, USA) *(UIST '12)*. ACM, New York, NY, USA, 319–326. https://doi.org/10.1145/2380116.2380157

[26] Jess McIntosh, Paul Strohmeier, Jarrod Knibbe, Sebastian Boring, and Kasper Hornbæk. 2019. Magnetips: Combining Fingertip Tracking and Haptic Feedback for Around-Device Interaction. In *Proceedings of the 2019 CHI Conference on Human Factors in Computing Systems* (Glasgow, Scotland Uk) *(CHI '19)*. Association for Computing Machinery, New York, NY, USA, 1–12. https://doi.org/10.1145/3290605.3300638

[27] Masa Ogata. 2018. Magneto-Haptics: Embedding Magnetic Force Feedback for Physical Interactions. In *Proceedings of the 31st Annual ACM Symposium on User Interface Software and Technology* (Berlin, Germany) *(UIST '18)*. ACM, New York, NY, USA, 737–743. https://doi.org/10.1145/3242587.3242615

[28] Farshid Salemi Parizi, Eric Whitmire, and Shwetak Patel. 2019. AuraRing: Precise Electromagnetic Finger Tracking. *Proc. ACM Interact. Mob. Wearable Ubiquitous Technol.* 3, 4, Article 150 (Dec. 2019), 28 pages. https://doi.org/10.1145/3369831

[29] Keunwoo Park, Daehwa Kim, Seongkook Heo, and Geehyuk Lee. 2020. MagTouch: Robust Finger Identification for a Smartwatch Using a Magnet Ring and a Built-in Magnetometer. In *Proceedings of the 2020 CHI Conference on Human Factors in Computing Systems* (Honolulu, HI, USA) *(CHI '20)*. Association for Computing Machinery, New York, NY, USA, 1–13. https://doi.org/10.1145/3313831.3376234

[30] Fabrizio Pece, Juan Jose Zarate, Velko Vechev, Nadine Besse, Olexandr Gudozhnik, Herbert Shea, and Otmar Hilliges. 2017. MagTics: Flexible and Thin Form Factor Magnetic Actuators for Dynamic and Wearable Haptic Feedback. In *Proceedings of the 30th Annual ACM Symposium on User Interface Software and Technology* (Québec City, QC, Canada) *(UIST '17)*. Association for Computing Machinery, New York, NY, USA, 143–154. https://doi.org/10.1145/3126594.3126609

[31] P. Smaragdis and J. C. Brown. 2003. Non-negative matrix factorization for polyphonic music transcription. In *2003 IEEE Workshop on Applications of Signal Processing to Audio and Acoustics (IEEE Cat. No.03TH8684)*. 177–180. https://doi.org/10.1109/ASPAA.2003.1285860

[32] A. Solin, M. Kok, N. Wahlström, T. B. Schön, and S. Särkkä. 2018. Modeling and Interpolation of the Ambient Magnetic Field by Gaussian Processes. *IEEE Transactions on Robotics* 34, 4 (2018), 1112–1127.

[33] J. F. Vasconcelos, G. Elkaim, C. Silvestre, P. Oliveira, and B. Cardeira. 2011. Geometric Approach to Strapdown Magnetometer Calibration in Sensor Frame. *IEEE Trans. Aerospace Electron. Systems* 47, 2 (2011), 1293–1306.

[34] Chang Xiao, Karl Bayer, Changxi Zheng, and Shree K. Nayar. 2019. Vidgets: Modular Mechanical Widgets for Mobile Devices. *ACM Trans. Graph.* 38, 4, Article 100 (July 2019), 12 pages. https://doi.org/10.1145/3306346.3322943

[35] Wataru Yamada, Hiroyuki Manabe, and Daizo Ikeda. 2018. CamTrackPoint: Camera-Based Pointing Stick Using Transmitted Light through Finger. In *Proceedings of the 31st Annual ACM Symposium on User Interface Software and Technology* (Berlin, Germany) *(UIST '18)*. Association for Computing Machinery, New York, NY, USA, 313–320. https://doi.org/10.1145/3242587.3242641

[36] Kentaro Yasu. 2017. Magnetic Plotter: A Macrotexture Design Method Using Magnetic Rubber Sheets. In *Proceedings of the 2017 CHI Conference on Human Factors in Computing Systems* (Denver, Colorado, USA) *(CHI '17)*. Association for Computing Machinery, New York, NY, USA, 4983–4993. https://doi.org/10.1145/3025453.3025702

[37] Kentaro Yasu. 2019. Magnetact: Magnetic-Sheet-Based Haptic Interfaces for Touch Devices. In *Proceedings of the 2019 CHI Conference on Human Factors in Computing Systems* (Glasgow, Scotland Uk) *(CHI '19)*. Association for Computing Machinery, New York, NY, USA, 1–8. https://doi.org/10.1145/3290605.3300470

[38] Kentaro Yasu. 2020. MagneLayer: Force Field Fabrication by Layered Magnetic Sheets. In *Proceedings of the 2020 CHI Conference on Human Factors in Computing Systems* (Honolulu, HI, USA) *(CHI '20)*. Association for Computing Machinery, New York, NY, USA, 1–9. https://doi.org/10.1145/3313831.3376552

[39] Sang Ho Yoon, Ke Huo, and Karthik Ramani. 2016. TMotion: Embedded 3D Mobile Input Using Magnetic Sensing Technique. In *Proceedings of the TEI '16: Tenth International Conference on Tangible, Embedded, and Embodied Interaction* (Eindhoven, Netherlands) *(TEI '16)*. ACM, New York, NY, USA, 21–29. https://doi.org/10.1145/2839462.2839463

[40] Sang Ho Yoon, Yunbo Zhang, Ke Huo, and Karthik Ramani. 2016. TRing: Instant and Customizable Interactions with Objects Using an Embedded Magnet and a Finger-Worn Device. In *Proceedings of the 29th Annual Symposium on User Interface Software and Technology* (Tokyo, Japan) *(UIST '16)*. ACM, New York, NY, USA, 169–181. https://doi.org/10.1145/2984511.2984529

[41] Zalmai, N., Kaeslin, C., Bruderer, L., Neff, S., and Loeliger, H. 1999. Gesture recognition from magnetic field measurements using a bank of linear state space models and local likelihood filtering. In *Proc. ICASSP '15*. 2569–2573.

[42] Clement Zheng, Jeeeun Kim, Daniel Leithinger, Mark D. Gross, and Ellen Yi-Luen Do. 2019. Mechamagnets: Designing and Fabricating Haptic and Functional Physical Inputs with Embedded Magnets. In *Proceedings of the Thirteenth International Conference on Tangible, Embedded, and Embodied Interaction* (Tempe, Arizona, USA) *(TEI '19)*. ACM, New York, NY, USA, 325–334. https://doi.org/10.1145/3294109.3295622